2019 MERIT self-directed joint research

Topological Kagome magnet $Co_3Sn_2S_2$ thin flakes with high electron mobility grown by chemical vapor transport and large anomalous Hall effect

Yukako Fujishiro and Miuko Tanaka
Department of Applied physics

Authors

Yukako Fujishiro: She studies synthesis of topological magnetic systems and transport measurement in Tokura group. In this joint research, she was responsible for crystal synthesis and transport measurement.

Miuko Tanaka: She studies transport property of van der Waals materials and their heterostructure in Nakamura group. In this joint research, she was responsible for device fabrication for the thin flakes.

Abstract

Magnetic Weyl semimetals attract considerable interest not only for their topological quantum phenomena but also as an emerging materials class for realizing quantum anomalous Hall effect in the two-dimensional limit. A shandite compound $Co_3Sn_2S_2$ with layered Kagome-lattices is one such material, where vigorous efforts have been devoted to synthesize the two-dimensional crystal. Here we report a synthesis of $Co_3Sn_2S_2$ thin flakes with a thickness of 250 nm by chemical vapor transport method. We find that this facile bottom-up approach allows the formation of large-sized $Co_3Sn_2S_2$ thin flakes of high-quality, where we identify the largest electron mobility (~2,600 cm2V-1s-1) among magnetic topological semimetals, as well as the large anomalous Hall conductivity (~1,400 W-1cm-1) and anomalous Hall angle (~32 %) arising from the Berry curvature. Our study provides a viable platform for studying high-quality thin flakes of magnetic Weyl semimetal and stimulates further research on unexplored topological phenomena in the two-dimensional limit.

This work was published in Nano Letters. [DOI: 10.1021/acs.nanolett.0c02962]

Introduction

Magnetic Weyl semimetals (WSMs) are materials that have non-degenerated Weyl points accompanied with the linear band structure around them due to a breaking of time reversal symmetry. The large anomalous Hall conductivity and anomalous Hall angle at zero magnetic field are known to be the hallmarks of diverging Berry curvature at the Weyl points in the presence of intrinsic magnetism [2]. In addition, they can potentially realize the quantum anomalous Hall effect (QAHE) in the two-dimensional (2D) limit [3]. If the intrinsic

magnetism realizes a large gap with a high magnetic ordering temperature, the QAHE may occur at a higher temperature than previous reports in doped magnetic topological insulators [7,8], offering versatile applications ranging from dissipationless electronics to topological quantum computing.

A ferromagnetic shandite compound $Co_3Sn_2S_2$ has attracted particular interest to this end. $Co_3Sn_2S_2$ crystallizes in a rhombohedral space group R-3m (No. 166) [9], where magnetic Co atoms form a 2D Kagome lattice with an Sn atom at the center of the hexagon, which is sandwiched between two S layers (Fig. 1(a)). These [S-(Co_3Sn)-S] structures are further connected by the hexagonal Sn layers. In this compound, Weyl points exist close to the E_F with almost no interference from trivial bands, leading to the emergence of large anomalous Hall effect and the anomalous Hall angle [4-6]. In addition to the quasi-2D layered crystal structure as well as the simple semi-metallic band structure, the intrinsic magnetism with the high Curie temperature (Tc ~ 180 K) makes it an ideal platform for exploring high-temperature QAHE.

Recently, there has been much effort devoted to the synthesis of 2D crystals of $Co_3Sn_2S_2$ from various approaches. In addition to the top-down method of microstructure fabrication using a focused ion beam (thickness ~350 nm) [10], the bottom-up approach such as the thin-film growth by molecular beam epitaxy (MBE) (thickness ~ 18 nm) [11] or sputtering deposition (thickness ~35 nm) [12] has been reported. However, the quality or uniformity of the thin film is limited. While the QAHE is expected only in the 2D limit (less than three unit-cells), it would be important to establish various feasible approaches to synthesize 2D crystals of $Co_3Sn_2S_2$ of high-quality, which may allow us to study the non-trivial crossover behaviors of topological transport properties from the bulk state towards the 2D limit.

Here we report an alternative bottom-up method for growing thin crystals of $Co_3Sn_2S_2$ using chemical vapor transport (CVT). While the CVT method is commonly used as bulk crystal growth approach, it can also be extended to the fabrication of single-crystalline nanoflakes, as demonstrated in several layered materials including transition metal dichalcogenides [13-15]. Compared to the thin film growth by vapor deposition of each element, the CVT method may potentially realize more high-crystalline and uniform sample by using the target material as a vapor source. In this work, we report the successful synthesis of high-quality $Co_3Sn_2S_2$ thin flakes with a thickness of 250 nm, exhibiting high electron mobility (~2,600 cm2V-1s-1) as well as large anomalous Hall effect (AHE) comparable or larger than those in bulk samples. The emergence of the high electron mobility and the large AHE is discussed in terms of the possible hole-doping in the thin flake, which is corroborated by variation of carrier density estimated from the band structure calculations.

Experiments

1, Thin flake growth by chemical vapor transport

We grew $Co_3Sn_2S_2$ thin flakes with the CVT method as schematically illustrated in Fig. 1(b). The source material was the milled powder of single-crystalline $Co_3Sn_2S_2$ grown by the Bridgman method, which was sealed in an evacuated quartz tube with iodine added as a transport agent. Then, the growth of the thin flakes was performed in a temperature gradient from 950 ℃ to 850 ℃ for 120 hours.

2, Fabrication of electrodes

The thin flakes formed at the inner surface of the quartz tube were picked up by the thermal release tape and subsequently released onto the SiO_2/Si substrate upon heating at 120 ℃ (Fig. 1(c)). The as-grown thin flakes with a thickness of 50 - 250 nm were formed at a high density as observed by optical microscopy (Figs. 1(d)-(f)), where the thickness was identified by atomic force microscopy (AFM). After transferring thin flakes on to the substrate, we directly deposited 600 nm-thick gold by electron beam evaporators, since we found that coating e-beam resist affected the flack surface and made it impossible to make an electrical contact. Then, the electrodes in a Hall bar geometry were patterned onto the thin flake through electron beam lithography with poly methyl methacrylate (PMMA) as an etching mask for the subsequent wet-etching process. The etching of gold was performed by immersing in undiluted potassium iodine for 44 seconds. After cleaning the sample with running purified water for ~7 minutes, the PMMS resist was removed by immersing in acetone.

3, Electron transport measurement

Magneto-transport measurements were performed in a Quantum Design PPMS with a standard four-probe method. The magnetic field was applied along the *c*-axis of the sample and perpendicular to the electric current. The longitudinal conductivity (σ_{xx}) and the Hall conductivity (σ_{xy}) were calculated as $\sigma_{xx} = \rho_{xx}/(\rho_{xx}^2 + \rho_{yx}^2)$ and $\sigma_{xy} = \rho_{yx}/(\rho_{xx}^2 + \rho_{yx}^2)$. Here, ρ_{xx} and ρ_{yx} are the longitudinal and Hall resistivity, respectively. The fitting by the two-carrier Drude model was applied to obtain mobilities and carrier densities at low temperature: $\sigma_{xy} = \frac{\mu_e^2 n_e eB}{1+\mu_e^2 B^2} + \frac{\mu_h^2 n_h eB}{1+\mu_h^2 B^2}$. Here, μ_e and μ_h represent mobility of electron and hole, respectively, while n_e and n_h represent the carrier density of electron and hole, respectively.

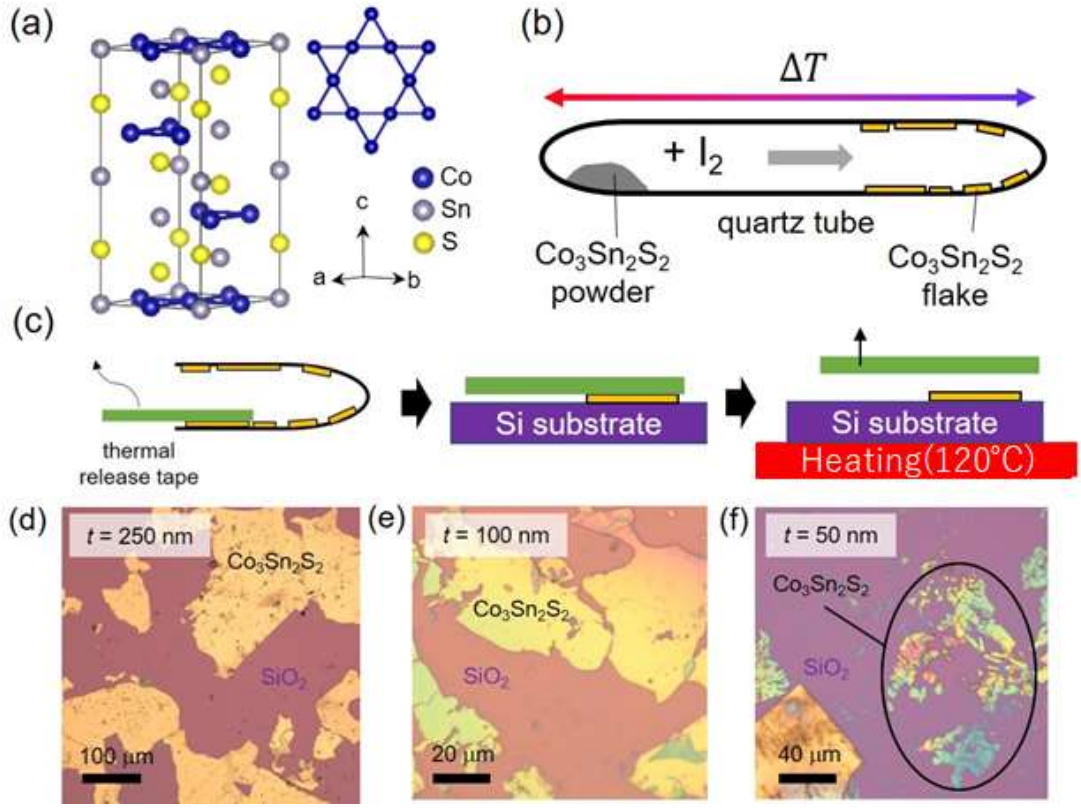

Fig. 1: (a) Crystal structure of $Co_3Sn_2S_2$. (b) A schematic of chemical vapor transport. (c) Transferring thin flakes onto Si/SiO_2 substrate. (d-f) Optical microscope images of thin flakes.

Result and discussion

Figure 2(b) shows the temperature (T) dependence of longitudinal resistivity (ρ_{xx}) of the thin flake (blue line) and the bulk single crystal grown by the Bridgman method (black line), which exhibit the kink structure at $T_c \sim 181$ K (thin flake) and $T_c \sim 173$ K (bulk sample). The observed residual resistivity ($\rho_{2K} \sim 23$ μΩcm) for the thin flake is smaller than that of the bulk sample ($\rho_{2K} \sim 91$ μΩcm) or those in previous studies [4,5,16], suggesting that the thin flake has high sample quality with few disorders. We also observed large non-saturating magnetoresistance (MR) reaching ~180 % at perpendicular magnetic field of $B = 14$ T at $T = 2$ K in the thin flake (Fig. 2(c)). Here, MR is defined as $[(\rho_{xx}(B) - \rho_{xx}(0)]/\rho_{xx}(0)$ where $\rho_{xx}(B)$ is the longitudinal resistivity in an applied magnetic field B. The observed large MR in the thin flake cannot be fully explained by the electron-hole compensation mechanism and requires further investigations. In addition, the thin flake shows a large coercive field (H_c) which is enhanced by a factor of 18 at $T = 2$ K ($\mu_0 H_c = 5.5$ T) compared to that in bulk samples ($\mu_0 H_c = 0.3$ T) (Fig. 2(d)). The similar enhancement of the coercivity has been also reported for $Co_3Sn_2S_2$ thin films [11,12].

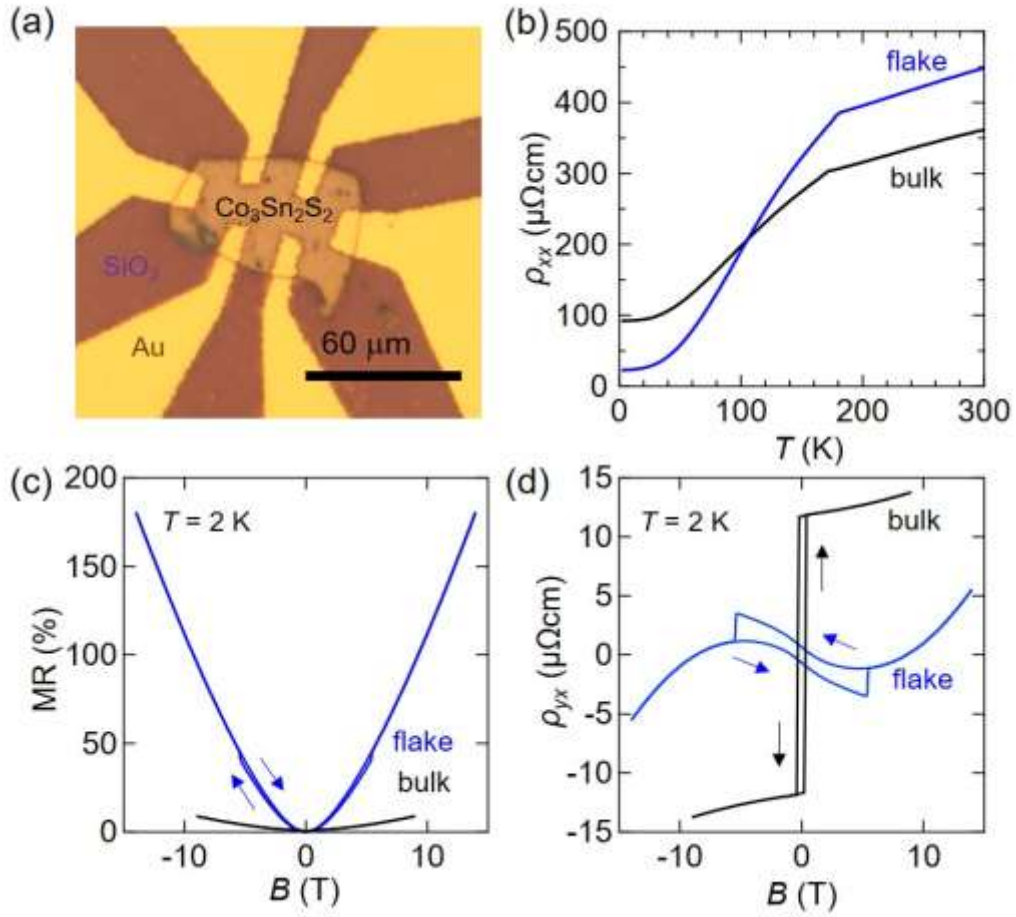

Fig. 2: (a) Optical microscope image of the 6 terminals device. (b) Temperature dependence of the longitudinal resistance at zero magnetic field. (c,d) Perpendicular magnetic field dependence of longitudinal (c) and Hall (d) resistance at 2 K.

Figure 3(a) shows the B-dependence of the Hall conductivity (σ_{xy}) measured at various temperatures for the 250 nm-thick flake. At T = 140 K, σ_{xy} exhibits a rectangular hysteresis loop with a sharp magnetization reversal associated with the AHE. While the AHE (the yellow shaded region in Fig. 3(a)) is almost constant for the variation of B at T = 140 K, a field-nonlinear behavior becomes pronounced upon lowering the temperature, which we assign to the normal Hall effect (NHE). Such a notable non-linear behavior is absent in the bulk sample. To obtain the mobility and carrier density from the NHE, we fitted the σ_{xy} with a two-carrier Drude model, after subtracting the field-independent σ^{A}_{xy} [$=\sigma_{xy}(B=0\ \mathrm{T})$] value at every magnetic field point. As shown by the dashed line at T = 2 K in Fig. 2(a), the Drude fitting can well reproduce the nonlinear magnetic field profile of σ_{xy} with the parameter values: μ_e =2587 $\mathrm{cm^2V^{-1}s^{-1}}$, μ_h = 119 $\mathrm{cm^2V^{-1}s^{-1}}$, $n_e = 1.47\times10^{19}$ $\mathrm{cm^{-3}}$, and $n_h = 5.32\times10^{20}$ $\mathrm{cm^{-3}}$ (Table 1). Here, μ_e and μ_h are the mobility while n_e and n_h are the carrier density of electron and hole,

respectively. We note that such a coexistence of the AHE hysteresis loop and the dispersive-resonance profile of the NHE has been rarely observed; indeed, the electron mobility observed here is the largest value ever reported for topological semimetals with intrinsic magnetism (*e.g.*, GdPtBi (~1,500 $cm^2V^{-1}s^{-1}$) [17], $MnBi_2Te_4$ flake (~1,100 $cm^2V^{-1}s^{-1}$) [18], Co_2MnGa (~35 $cm^2V^{-1}s^{-1}$) [19]), suggesting a presence of small electron pockets in addition to the high sample quality of the thin flake.

The T dependence of the σ^A_{xy} taken at $B = 0$ T and the anomalous Hall angle defined as $\sigma^A_{xy}/\sigma_{xx}$ are shown in Fig. 3(b), where σ_{xx} is the longitudinal conductivity. The σ^A_{xy} reaching ~1,400 $\Omega^{-1}cm^{-1}$ is nearly independent of temperature below $T = 160$ K, which suggests the Berry-curvature mechanism. The observed σ^A_{xy} is comparable or slightly enhanced compared to those in previous studies, which reported the σ^A_{xy} of 500−1,400 $\Omega^{-1}cm^{-1}$ [4,5,10,11,16]. Accordingly, the large anomalous Hall angle reaching ~ 32 % around $T = 140$ K was identified in the thin flake. To investigate the possible extrinsic contributions to the AHE, we adopted the established scaling relation between ρ_{xx} and ρ_{yx} for the AHE [10]. The Hall resistivity at zero magnetic field can be written as $\rho_{yx} = \left(\alpha\rho_{xx} + \beta\rho_{xx}^2\right) \cdot M$, where the first term represents the skew-scattering while the second term corresponds to the sum of side-jump and intrinsic contributions. Both parts are linearly proportional to magnetization (M). Hence, the linear fitting for $\rho_{yx}/\rho_{xx}M$ against ρ_{xx} gives the parameters α (intercept) and β (slope). As shown in Fig. 3(c), the linear fitting reveals small contribution from the skew-scattering (less than -160 $\Omega^{-1}cm^{-1}$), being consistent with the previous reports in bulk samples [5,20].

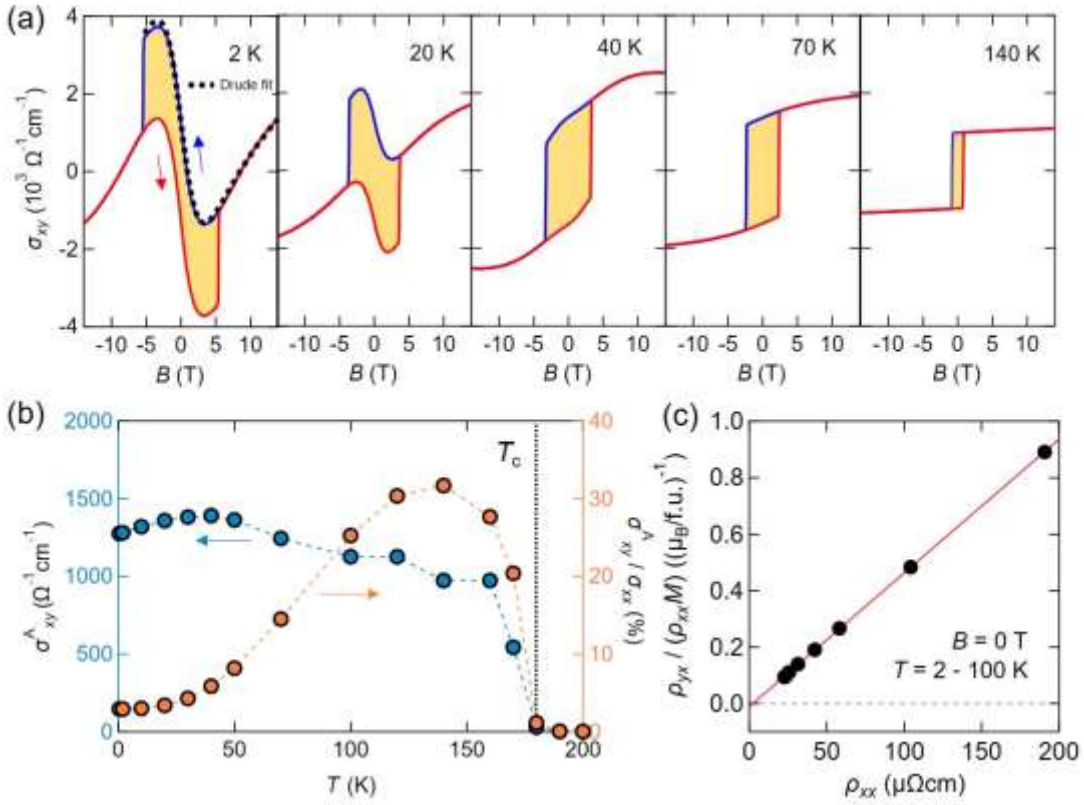

Fig. 3: (a)Magnetic field dependence of the Hall conductivity. (b) Temperature dependence of anomalous Hall conductivity and anomalous Hall angle. (c) Scaling relationship of Hall resistivity. The slope indicate contribution from side-jump and intrinsic, and the intercept indicate contribution from skew-scattering. We use the magnetization M value measured in bulk crystal.

$Co_3Sn_2S_2$	μ_e (cm²/Vs)	μ_h (cm²/Vs)	n_e (/cm³)	n_h (/cm³)	Ref
bulk (flux)	730	640	7.6×10^{19}	9.3×10^{19}	[4]
bulk (CVT)	1796	1768	8.4×10^{19}	8.8×10^{19}	[20]
bulk (Bridgman)	574	532	5.3×10^{19}	4.7×10^{19}	This work
thin flake (CVT)	2579	155	1.5×10^{19}	3.4×10^{20}	

Table 1: Mobility and carrier density in this work and previous reports. Temperature is 2 K in all the measurement.

To understand the emergence of high electron mobility as well as the large intrinsic AHE in a comprehensive way, we requested Prof. Koretsune, Prof. Arita, and Dr Minami for

the band structure calculations of $Co_3Sn_2S_2$ (Fig. 4(a)). The electronic band structure of $Co_3Sn_2S_2$ without the spin-orbit coupling (SOC) has two sets of linear band crossing points of the nodal ring along the Γ－L and L－U paths, which are located slightly above and below the E_F, respectively. The Weyl points appear at 60 meV above the E_F by including the SOC, while the nodal ring forms a gap due to anti-crossings (the inset of Fig. 4(a)). In undoped samples, the carrier density as well as the mobility for electron and hole become roughly equal as reported in bulk samples (Table 1) [4,16]. On the other hand, the reduction(enhancement) of electron(hole) carrier density or the enhancement(reduction) of electron(hole) mobility observed in the thin flake (Table 1) can be attributed to the effective process of hole-doping (Fig. 4b). Indeed, the observed carrier density is consistent with the calculated values for the E_F shift by about -30 meV or the change in electron(hole) density by ~1.4×10^{20} cm^{-3} (~3.5×10^{20} cm^{-3}) (Fig. 4(b)). The reason for the possible hole-doping remains unclear at this moment, and further exploration of the synthesis conditions for CVT and device fabrication process would be necessary to reveal its origin. At the same time, we find that the calculated σ^A_{xy} (Fig. 4(c)) shows the enhancement in the hole-doping region, with a maximum point locating around the E_F shift by ~20 meV or the increase of the hole density by ~1.6×10^{20} cm^{-3}, which corroborates our observation of the large AHE being comparable or slightly enhanced than in undoped bulk samples. In the meanwhile, the reason why the observed σ^A_{xy} in the thin flake is even larger than that of the calculated value (1,150 $\Omega^{-1}cm^{-1}$) remains elusive. We found that that electronic structure of $Co_3Sn_2S_2$ with a thickness larger than ~10 nm should be identical to that of the bulk limit, and hence there should not be a modification of the bulk electronic structure in the 250 nm-thick sample discussed in this work. We speculate that there may be some non-trivial effects from the surface or domain wall conductions. Systematic investigations in thinner flakes would be imperative to reveal such a possibility.

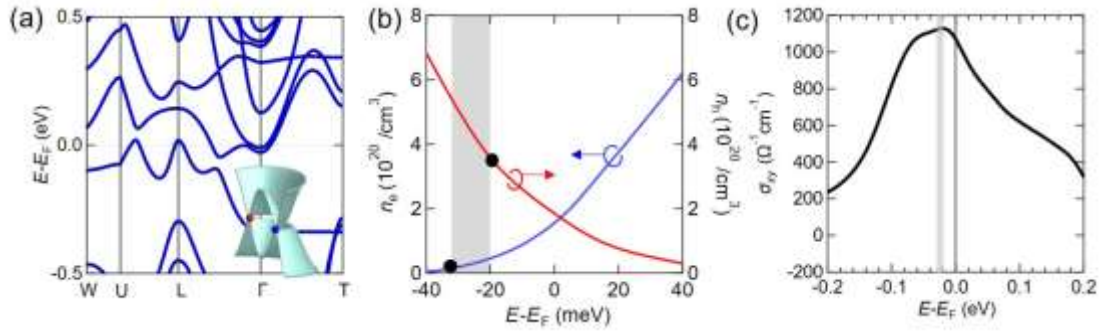

Fig. 4: (a) Band structure calculation assuming SOC and experimentally determined lattice constant. (b) Energy dependence of carrier density. (c) Energy dependence of anomalous Hall conductivity.

Summary

We have established an accessible arena for studying high-quality $Co_3Sn_2S_2$ thin flakes by using the CVT method. Towards the synthesis of even thinner flakes, it would be important to optimize the growth parameters of CVT. The CVT-grown thin flake exhibited the highest mobility among topological semimetals with intrinsic magnetism, as well as the large intrinsic AHE arising from the Berry curvature. These results suggest the high sample quality and uniformity of the thin flake, which would be important for studying exotic quantum phenomena of the magnetic Weyl semimetal in reduced dimensionality, and paves the way for the realization of high-temperature QAHE in the 2D limit.

Acknowledgement

We appreciate Prof. Tokura, Prof. Nakamura, Prof. Kanazawa, and Dr. Mogi in u-Tokyo, Prof. Tarucha, and Prof. Yamamoto in RIKEN, for fruitful advices. We appreciate Dr. Kaneko for helping us on CVT growth, and Mr. Yokosawa for advice on device fabrication. We also appreciate Dr. Minami, Prof. Koretsune, and Prof. Arita for band calculation.

We are grateful to Prof. Shibauchi, Prof. Shimano, and MERIT program for giving us a great opportunity for the joint research.

References

[1] Armitage, N. P., Mele, E. J. & Vishwanath, A. Weyl and Dirac semimetals in three-dimensional solids. *Rev. Mod. Phys.* **90**, 015001 (2018)

[2] Nagaosa, N., Sinova, J., Onoda, S., MacDonald, A. H. & Ong, N. P. Anomalous Hall effect, *Rev. Mod. Phys.* **82**, 1539 (2010)

[3] Xu, G., Weng, H., Wang, Z., Dai, X. & Fang, Z. Chern semimetal and the quantized anomalous Hall effect in $HgCr_2Se_4$, *Phys. Rev. Lett.* **107**, 186806 (2011)

[4] Liu, E. *et al.* Giant anomalous Hall effect in a ferromagnetic kagome-lattice semimetal. *Nat. Phys.* **14**, 1125 (2018)

[5] Wang, Q. e*t al.* Large intrinsic anomalous Hall effect in half-metallic ferromagnet $Co_3Sn_2S_2$ with magnetic Weyl fermions. *Nat. Commun.* **9**, 3681 (2018)

[6] Liu, D. F. *et al.* Magnetic Weyl semimetal phase in a Kagomé crystal. *Science* **365**, 1282 (2019)

[7] Yu, R. e*t al.* Quantum anomalous Hall effect in magnetic topological insulators. *Science* **329**, 5987 (2010)

[8] Chang, C. -Z. e*t al.* Experimental observation of the quantum anomalous Hall effect in a magnetic topological insulator. *Science* **340**, 167 (2013)

[9] Weihrich, R. & Anusca, I & Zabel, M. Half-antiperovskites: Structure and type-antitype relations of Shandites $M_{3/2}AS$ (M = Co, Ni; A = In, Sn). *Z. Anorg. Allg. Chem.* **631**, 1463 (2005)

[10] Geishendorf, K. *et al.* Magnetoresistance and anomalous Hall effect in micro-ribbons of the magnetic

Weyl semimetal $Co_3Sn_2S_2$. *Appl. Phys. Lett.* **114**, 092403 (2019)

[11] Li, S. *et al.* Epitaxial growth and transport properties of magnetic Weyl semimetal $Co_3Sn_2S_2$ thin films. *ACS Appl. Electron. Mater.* **2**, 126 (2020)

[12] Fujiwara, K. *et al.* Ferromagnetic $Co_3Sn_2S_2$ thin films fabricated by co-sputtering. *Jpn. J. Appl. Phys.* **58**, 050912 (2019)

[13] Wang, J. *et al.* Controlled synthesis of two-dimensional 1T-$TiSe_2$ with charge density wave transition by chemical vapor transport. *J. Am. Chem. Soc.* **138**, 16216 (2016)

[14] Hu, D. *et al.* Two-dimensional semiconductor grown by chemical vapor transport. *Angew. Chem. Int. Ed.* **56**, 1 (2017)

[15] Grönke, M. *et al.* Chemical vapor growth and delamination of α-$RuCl_3$ nanosheets down to the monolayer limit. *Nanoscale.* **10**, 19014 (2018)

[16] Ding, L. *et al.* Intrinsic anomalous Nernst effect amplified by disorder in a half-metallic semimetal. *Phys. Rev. X.* **9**, 041061 (2019)

[17] Hirschberger, M. *et al.* The chiral anomaly and the thermopower of Weyl fermions in the half-Heusler GdPtBi. *Nat. Matter.* **15**, 1161 (2015)

[18] Lee, S. H. *et al.* Transport evidence for a magnetic-field induced ideal Weyl state in antiferromagnetic topological insulator $Mn(Bi_{1-x}Sb_x)_2Te_4$. arXiv:2002.10683

[19] Belopolski, I. *et al.* Discovery of topological Weyl fermion lines and drumhead surface states in a room temperature magnet. *Science* **365**, 1278 (2019)

[20] Zhou, H. *et al.* Enhanced anomalous Hall effect in the magnetic topological semimetal $Co_3Sn_{2-x}In_xS_2$. *Phys. Rev. B* **101**, 125121 (2020)